

Atherogenic region and diet diminish glycocalyx dimension and increase intima-to-media ratios at murine carotid artery bifurcation

Bernard M. van den Berg, Jos A. E. Spaan, Titia M. Rolf and Hans Vink

Am J Physiol Heart Circ Physiol 290:915-920, 2006. First published Sep 9, 2005;

doi:10.1152/ajpheart.00051.2005

You might find this additional information useful...

This article cites 22 articles, 13 of which you can access free at:

<http://ajpheart.physiology.org/cgi/content/full/290/2/H915#BIBL>

This article has been cited by 1 other HighWire hosted article:

Differential inhibition by hyperglycaemia of shear stress- but not acetylcholine-mediated dilatation in the iliac artery of the anaesthetized pig

R. Kelly, T. Ruane-O'Hora, M. I. M. Noble, A. J. Drake-Holland and H. M. Snow

J. Physiol., May 15, 2006; 573 (1): 133-145.

[\[Abstract\]](#) [\[Full Text\]](#) [\[PDF\]](#)

Updated information and services including high-resolution figures, can be found at:

<http://ajpheart.physiology.org/cgi/content/full/290/2/H915>

Additional material and information about *AJP - Heart and Circulatory Physiology* can be found at:

<http://www.the-aps.org/publications/ajpheart>

This information is current as of February 12, 2007 .

Atherogenic region and diet diminish glycocalyx dimension and increase intima-to-media ratios at murine carotid artery bifurcation

Bernard M. van den Berg, Jos A. E. Spaan, Titia M. Rolf, and Hans Vink

Department of Medical Physics, Academic Medical Center, University of Amsterdam, Amsterdam, The Netherlands

Submitted 18 January 2005; accepted in final form 6 September 2005

van den Berg, Bernard M., Jos A. E. Spaan, Titia M. Rolf, and Hans Vink. Atherogenic region and diet diminish glycocalyx dimension and increase intima-to-media ratios at murine carotid artery bifurcation. *Am J Physiol Heart Circ Physiol* 290: H915–H920, 2006. First published September 9, 2005; doi:10.1152/ajpheart.00051.2005.—It was hypothesized that endothelial glycocalyx perturbation contributes to increased vulnerability of the arterial wall exposed to atherogenic risk factors. Glycocalyx and intima-to-media ratios (IMR) were studied at a low- and a high-risk region within the murine carotid artery (common region) and internal carotid branch (sinus region) in control C57BL/6J (C57BL6) and age-matched C57BL/6J/apoE*3-Leiden (apoE*3; on an atherogenic diet) mice. Electron micrographs revealed significantly thinner glycocalyces [73 (SD 36) vs. 399 (SD 174) nm, $P < 0.05$] and greater IMR [0.096 (SD 0.045) vs. 0.044 (SD 0.023), $P < 0.05$] at the sinus region of C57BL6 mice than in the common region. Thinner glycocalyces [100 (SD 27) vs. 399 (SD 174) nm, $P < 0.05$] and greater IMR [0.071 (SD 0.024) vs. 0.044 (SD 0.023), $P < 0.05$] were also observed in the common region of age-matched apoE*3 mice on an atherogenic diet for 6 wk vs. C57BL6 mice on a normal diet. Greater IMR were due to greater intima layers, without significant changes in media layer dimension. In addition, atherogenic diet resulted in increased endothelial cell thickness at the sinus region [0.85 (SD 0.49) vs. 0.53 (SD 0.28) μm , $P < 0.05$] but not at the common region [0.66 (SD 0.37) vs. 0.62 (SD 0.32) μm]. It is concluded that both regional and diet-induced increases in atherogenic risk are associated with smaller glycocalyx dimensions and greater IMR and that vascular sites with diminished glycocalyx are more vulnerable to proinflammatory and atherosclerotic sequelae.

flow; permeability

THE IMPORTANCE of an endothelial cell surface glycocalyx has been established by functional studies and electron microscopic observations. The endothelial glycocalyx shields the vascular wall from flowing blood, limits leakage of fluid and macromolecules across its endothelial lining, forms a mechanical barrier against adhesion of leukocytes and platelets to the endothelial surface, and stimulates endothelial NO release by mechanotransducing fluid shear stresses (3–5, 15, 21, 23). Although reduced levels of surface-bound sialic acids (9) and increased endothelial permeability and susceptibility to atherosclerotic lesion formation (10) have been found to coincide with arterial branch points and curvatures, little is known about the contribution of glycocalyx perturbation to the increased vascular vulnerability of high-atherogenic risk areas.

Atherosclerotic lesions within the arterial tree develop at predictable vessel geometries, e.g., arterial branching and curvatures, and constraints on vessel motion by the surrounding tissues, which lead to local flow instabilities and separations

(24). Such lesions can be detected and visualized as changes in vascular wall properties and quantified as intima-to-media ratios (IMR). Increases in IMR have been found to be associated with increased cardiovascular risk factors and atherosclerosis (1, 17, 18).

We hypothesized that endothelial cells, which play a central role in response to shear stress (6), express a modified surface glycocalyx at high-atherogenic risk regions and, in turn, contribute to predisposition of these arterial sites to atherosclerotic lesion formation. In the present study, endothelial glycocalyx dimension was investigated at low- and high-risk regions of the C57BL/6J (C57BL6) mouse carotid artery, using the common and internal carotid bifurcation (sinus) area as a model for arterial sites exposed to low and high atherogenic risk, respectively (13). In addition, age-matched C57BL/6J/apoE*3-Leiden (apoE*3) mice received an atherogenic stimulus for a relatively short period of 6 wk to investigate its early effects on the endothelial glycocalyx. These transgenic apoE*3 mice contain a mutant human apoE gene that is associated with familial dyslipoproteinemia in humans and are a suitable model for different aspects of early atherogenesis when fed a high-fat, high-cholesterol diet (14, 22).

Electron microscopy on combined Alcian blue 8GX- and acridine orange-stained vessels was used to determine the endothelial glycocalyx thickness, IMR, and endothelial and subendothelial layer thickness in the common carotid and internal carotid regions in C57BL6 and apoE*3 mice.

MATERIALS AND METHODS

Mice. Male C57BL6 ($n = 6$) and apoE*3 ($n = 6$) mice were used. Transgenic apoE*3 mice expressing the human apoE*3-Leiden gene were generated and bred with C57BL6 females as described earlier (22), and the F₁₀ generation was used. Mice were kept on standard mouse chow (SRM-A; Hope Farms, Woerden, The Netherlands) until, at the age of 8 wk, apoE*3 mice were put on a diet containing 15% cacao butter, 0.5% cholate, 1% cholesterol, 40.5% sucrose, 10% corn starch, 1% corn oil, and 4.7% cellulose (Diet-N; Hope Farms) for 6 wk (16).

Cholesterol and triglyceride serum levels were determined ($n = 6$ /group) from blood collected by saphenous vein puncture (10) with a MPR2 cholesterol kit (Boehringer Mannheim) and a GPO-Trinder kit (Sigma-Aldrich), respectively.

Perfusion and tissue preparation. The experimental protocol was approved by the local Animal Ethical Committee (DEC) of the Academic Medical Center at the University of Amsterdam. Fourteen-week-old male C57BL6 and apoE*3 mice received an intraperitoneal dose of 125 mg/kg ketamine HCl (Nimatek; Eurovet, Bladel, The Netherlands) and 0.2 mg medetomidine HCl (Orion, Espoo, Finland). The abdominal aorta and vena cava of anesthetized mice [24.9 (SD

Address for reprint requests and other correspondence: H. Vink, Dept. of Medical Physics, Academic Medical Center, Univ. of Amsterdam, Meibergdreef 15, 1105 AZ, Amsterdam, The Netherlands (e-mail: h.vink@amc.uva.nl).

The costs of publication of this article were defrayed in part by the payment of page charges. The article must therefore be hereby marked "advertisement" in accordance with 18 U.S.C. Section 1734 solely to indicate this fact.

1.4) and 22.0 (SD 3.4) g, respectively] were ligated cranial to the iliac artery bifurcation. The abdominal aorta was cannulated in retrograde caudal to the left renal artery branch, and perfusion was started with oxygenated HEPES-buffered salt solution (in mmol/l: 5.55 glucose, 114 NaCl, 10 KCl, 1.18 KH_2PO_4 , 1.17 $\text{MgSO}_4 \cdot 7\text{H}_2\text{O}$, 0.5 CaCl_2 , 25 NaHCO_3 , 5.0 HEPES, 0.025 EDTA) containing 0.1% bovine serum albumin and 5 IU/ml heparin (pH 7.4, 37°C) at 2 ml/min [23 (SD 3.9) and 22 (SD 7.7) mmHg, respectively]. Both left and right external jugular veins were cut to create an outflow, and perfusion continued for 10 min to remove the blood. Perfusion solution was changed to a phosphate-buffered fixative (pH 7.4) containing 15 mmol/l MgCl_2 at 2 ml/min, to which acridine orange and Alcian blue 8GX (Sigma, St. Louis, MO) were added after 2 min (final concentrations 0.01% and 0.05%, respectively), and perfusion continued for 30 min at room temperature [46 (SD 12) and 44 (SD 17) mmHg, respectively]. During perfusion, inflow of perfusion solutions was monitored continuously with an in-line flow probe and meter (Transonic Systems, Ithaca, NY) and recorded with a Powerlab/4sp (ADInstruments, Castle Hill, Australia). Application of a 2 ml/min flow in the abdominal aorta resulted in a left common carotid artery flow of 0.14 ml/min (SD 0.02) (C57BL6, $n = 5$), as measured with a 0.5-V B424 flow probe (Transonic) placed locally around the left common carotid artery.

After perfusion, the left common carotid artery plus internal and external carotid arteries were dissected as a whole ($n = 6/\text{group}$). After a further overnight fixation in 4% buffered formalin, the entire vessel segment was postfixed with 1% osmium tetroxide (Electron Microscopy Sciences, Fort Washington, PA) and 1% lanthanum nitrate (Sigma) in water for 2 h at room temperature, followed by 1% aqueous uranyl acetate for 1 h, and processed further for electron microscopy. The carotid artery preparation was positioned in such a way that allowed a longitudinal sectioning of both the common and internal carotid arteries as depicted in Fig. 1. Within the resulting sections, three regions were localized, corresponding to the common carotid artery (*region I*), the sinus region within the internal carotid artery (*region II*), and its opposite region, the flow divider site of the internal carotid artery (*region III*). Digital pictures from *regions I* and *II* (Fig. 1) of each 80-nm ultrathin section of the vessel wall were obtained with a built-in Megaview II charge-coupled device camera and processed with analySIS image analytical software (both from Soft Imaging Systems, Münster, Germany). Digital pictures of *region III* of sections from C57BL6 mice were also obtained as a control.

Data analysis. Pictures were analyzed with Image-Pro Plus software version 3.0 (Media Cybernetics, Silver Spring, MD). The number of micrographs per region of interest is indicated in Figs. 3 and 4 and Table 2. The micrographs cover $\sim 100 \mu\text{m}$ in length within these

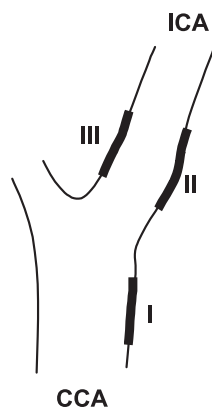


Fig. 1. Schematic drawing of longitudinal section of the common carotid artery (CCA) and internal carotid artery (ICA) segment depicting the regions used for measurement. *I*, common carotid region; *II*, internal carotid, sinus region; *III*, internal carotid, flow divider region.

regions. Endothelial surface glycocalyx thickness recorded at transmission electron microscopy (TEM) magnifications ($\times 1,040$) was measured at places within the depicted regions with a visible membrane double layer (confirmed at $\times 18,000$ or $\times 25,000$). Such sections of endothelial cells were considered to be cut perpendicular to the cell surface with an error of not more than $\pm 6^\circ$ (2). Mean endothelial surface glycocalyx thickness within the indicated carotid artery regions was determined to be the distance of stained structures between the luminal membrane of the endothelial cell and their luminal boundary, measured as the optical background density + 2SD. This represents $\sim 95\%$ of detectable length of the stained structures (21).

The IMR was determined to be the intimal thickness divided by the medial layer thickness. Intimal thickness, between vascular lumen and internal elastic lamina (19), was recorded at TEM magnification ($\times 1040$) and comprised both endothelial and subendothelial layers. Intimal thickness was determined by measured intimal area divided by intimal area midlength. Medial thickness, between internal and external elastic lamina, was determined accordingly.

Subendothelial matrix thickness, between endothelial basal membrane and internal elastic lamina, recorded at TEM magnifications ($\times 4,200$, $\times 18,000$, or $\times 25,000$), was determined by measured subendothelial matrix area divided by subendothelial matrix midlength. Endothelial cell layer thickness was determined accordingly.

Data are presented as means (SD). Differences in serum cholesterol and triglyceride levels between C57BL6 and apoE*3 mice were assessed by means of two-sample *t*-test (2 way). Differences in glycocalyx thickness and intima and endothelial cell layer thickness between carotid artery regions of C57BL6 and apoE*3 mice were assessed by means of two-sample *t*-test (2 way). Differences in intimal and medial thickness and IMR were assessed by paired-sample *t*-test (2 way). A value of $P < 0.05$ was considered statistically significant.

RESULTS

Glycocalyx dimensions in C57BL6 mice on normal diet.

Electron micrographs of the luminal surface of combined Alcian blue- and acridine orange-stained left internal carotid sinus region in C57BL6 mice revealed a thinner, condensed surface coat compared with the bushlike structures observed on the left common carotid artery surface (Fig. 2, *B* and *A*, respectively). Within the internal carotid sinus (*region II*) the endothelial glycocalyx of 73 (SD 36) nm was significantly smaller ($P < 0.05$) than the glycocalyx lining the common carotid artery (*region I*), measuring 399 (SD 174) nm (Fig. 3).

In addition, glycocalyx thickness was measured in the opposite site of the internal sinus region, the internal flow divider region (*region III*; Fig. 1). Whereas the sinus (*region II*) of the internal carotid artery is exposed to a disturbed laminar flow, the opposite site (*region III*) is supposed to be exposed to high undisturbed laminar flow profiles. Glycocalyx thickness in the flow divider region measures 308 (SD 185) nm, which is not different from the common carotid glycocalyx thickness.

*Glycocalyx dimensions in apoE*3 mice on atherogenic diet.*

An age-matched group of apoE*3 mice were put on a high-fat, high-cholesterol diet for 6 wk to induce systemic high cholesterol and triglyceride levels, a risk factor for atherosclerotic lesion formation. In this relatively short period, apoE*3 mice already had significantly higher serum cholesterol [47.5 (SD 6.53) vs. 3.1 (SD 0.53) mmol/l, $P < 0.05$] and triglyceride [2.0 (SD 0.85) vs. 0.8 (SD 0.16) mmol/l, $P < 0.05$] levels compared with C57BL6 mice on a normal diet (Table 1). Electron micrographs of the common carotid and internal carotid sinus

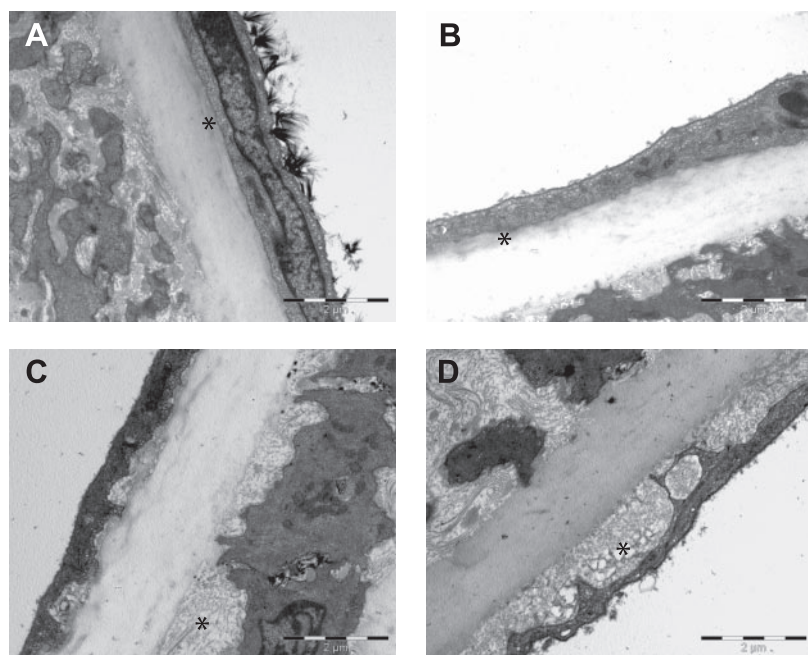


Fig. 2. Electron microscopic overview of Alcian blue 8GX-stained mouse left common carotid artery region (A and C) and internal carotid artery sinus region (B and D) of C57BL/6J or C57BL/6J/apoE*3-Leiden mice. Asterisk indicates the location of the subendothelial matrix layer within the vascular wall segment.

regions in these mice showed in both regions a thin condensed surface coat similar to the staining observed in C57BL6 mouse internal carotid sinus (Fig. 2, C and D, respectively). Glycocalyx dimension at the common carotid area [100 nm (SD 27)] was significantly reduced ($P < 0.05$) compared with mice on a normal diet. No significant change was observed in the dimension of the glycocalyx at the sinus area of the internal carotid artery branch [68 nm (SD 21); Fig. 3].

Intima-to-media ratios. Investigation of changes in vascular wall properties revealed a significant difference ($P < 0.05$) in IMR between the common carotid and internal carotid sinus regions of C57BL6 mice [0.044 (SD 0.023) and 0.096 (SD 0.045), respectively; Table 2]. Compared with mice on a normal diet, the IMR at the common carotid artery region of high-fat apoE*3 mice was significantly increased to 0.071 (SD

0.024) ($P < 0.05$). There was no significant effect of the atherogenic diet on IMR at the sinus area [0.190 (SD 0.303)]. In apoE*3 mice, IMR at the common carotid area remained significantly smaller than the sinus area IMR ($P < 0.05$).

Dimensions of intima and media layers. No significant differences were observed in the media layer thickness of the common and sinus areas of mice on normal and high-fat diets (Table 2). Consistent with the observed greater IMR at the sinus areas, the corresponding sinus area intima were thicker in normal-diet mice [1.45 (SD 0.65) vs. 0.79 (SD 0.30) μm , sinus area vs. common area; $P < 0.05$] and atherogenic-diet mice [2.85 (SD 4.01) vs. 1.01 (SD 0.42) μm , sinus area vs. common area; $P < 0.05$].

The thicker intima at the sinus regions were accompanied by significant swelling of the subendothelial matrix between endothelium and internal elastic lamina in normal-diet mice [347 (SD 167) vs. 136 (SD 61) nm, sinus area vs. common area; $P < 0.05$] as well as in atherogenic-diet mice [448 (SD 508) vs. 187 (SD 132) nm, sinus vs. common area; $P < 0.05$; Fig. 4]. Furthermore, the endothelial cell layer was significantly thicker in apoE*3 mice [851 (SD 489) and 658 (SD 366) nm, sinus and common area, respectively] compared with the endothelial thickness at the same areas in mice on a normal diet [527 (SD 276) and 617 (SD 316) nm, respectively].

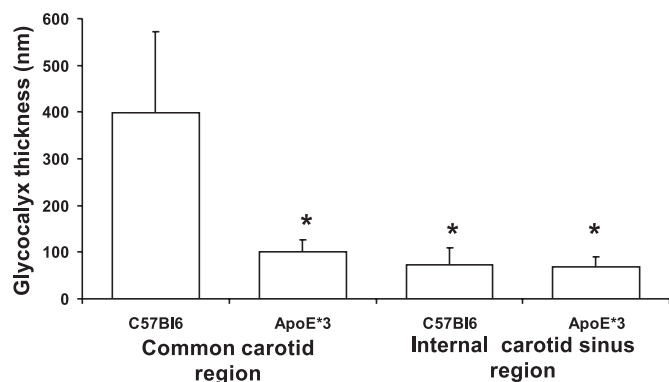


Fig. 3. Distribution of glycocalyx thickness measured within the common carotid artery region of C57BL/6J (C57BL6) and C57BL/6J/apoE*3-Leiden (apoE*3) mice (data from 18 and 26 micrographs, respectively) and the internal carotid artery sinus region of C57BL6 and apoE*3 mice (data from 18 and 20 micrographs, respectively). Values are means (SD). Difference in glycocalyx thickness between carotid artery regions of C57BL6 and apoE*3 mice was assessed by means of 2-sample *t*-test (2 way). * $P < 0.05$ vs. C57BL6, common carotid region.

Table 1. Serum cholesterol and triglyceride levels

Strain	Diet	<i>n</i>	Cholesterol, mmol/l	Triglycerides, mmol/l
C57BL6	NC	6	3.1 (0.53)	0.8 (0.16)
apoE*3	HFC	6	47.5 (6.53)*	2.0 (0.85)*

Results are means (SD) for *n* serum samples. Difference in serum cholesterol and triglyceride levels between C57BL/6J (C57BL6) and C57BL/6J/apoE*3-Leiden (apoE*3) mice was assessed by means of 2-sample *t*-test (2 way). NC, normal chow; HFC, high-fat chow. * $P < 0.05$ vs. C57BL6.

Table 2. Intimal and medial thickness and intima-to-media ratio of vascular wall within common carotid and internal carotid artery sinus of C57BL6 and apoE*3 mice

Mouse Region	<i>n</i>	Intimal Thickness,* μm	Medial Thickness, μm	Intima-to-Media Ratio*
C57BL6				
I	18	0.79 (0.30)	19.2 (3.6)	0.044 (0.023)
II	18	1.45 (0.65)	15.7 (3.9)	0.096 (0.045)
apoE*3				
I	26	1.01 (0.42)	14.3 (3.1)	0.071 (0.024)
II	20	2.85 (4.01)	18.0 (3.9)	0.190 (0.303)

Results are means (SD) for *n* micrographs. Difference in intimal and medial thickness and intima-to-media ratio between carotid artery regions of C57BL6 and apoE*3 mice was assessed by paired-sample *t*-test (2 way). **P* < 0.05 between regions I and II of C57BL6 and apoE*3 mice.

DISCUSSION

Main findings. In the present study we demonstrate that the dimension of the endothelial glycocalyx at the sinus region of the mouse internal carotid artery is significantly less than the glycocalyx dimension on the luminal surface of the common carotid artery. This finding supports the hypothesis that pertur-

bation of the glycocalyx contributes to the increased vascular vulnerability of regions that are at high atherogenic risk. Furthermore, this thinner glycocalyx is accompanied by greater IMR and a thicker subendothelial layer, confirming that regional differences in glycocalyx dimension reflect variations in its vasculoprotective capacity. In addition, we found that common carotid glycocalyx dimensions are reduced in an atherogenic mouse model put on a high-fat, high-cholesterol diet for 6 wk. In agreement, this atherogenic perturbation of the glycocalyx is again accompanied by increases in IMR and greater intima dimensions.

Mechanism of glycocalyx reduction at high-risk regions. The fact that glycocalyx dimension is significantly less at the sinus region than the glycocalyx dimensions at the opposite site of the internal carotid near the flow divider as well as at the common carotid area just proximal to the carotid bifurcation suggests that spatial differences in glycocalyx dimension are related to local variations in flow profiles. It is well known that areas of high atherogenic risk are located close to regions of disturbed flow at arterial bifurcations. Therefore, it is tempting to speculate that undisturbed flow patterns and the associated stimulation of vascular endothelium by fluid shear stress are essential to obtain optimal glycocalyx protective properties.

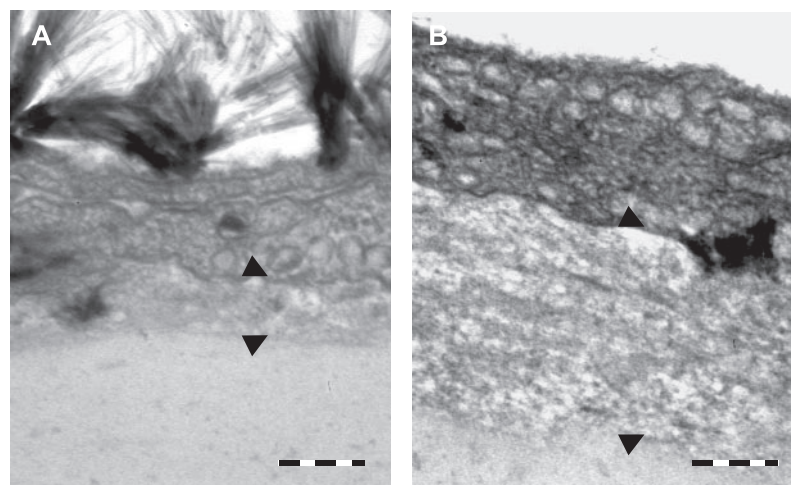
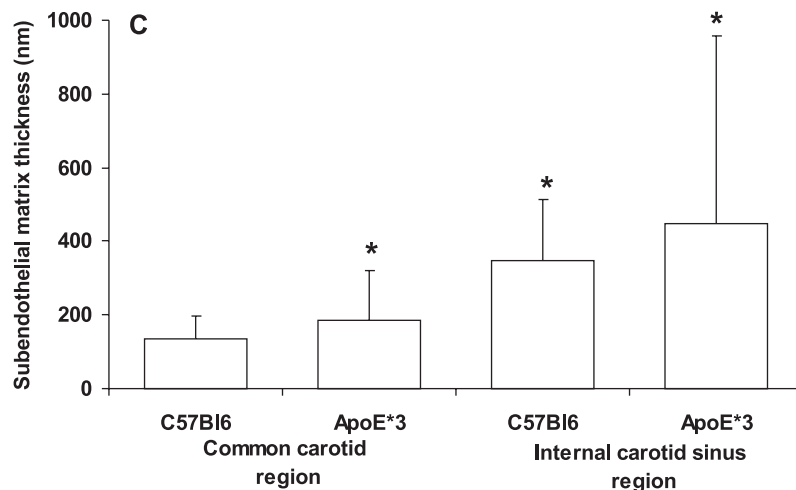


Fig. 4. Electron microscopic detail of Alcian blue 8GX-stained normal diet C57BL6 mouse left common carotid (A) and internal carotid (B) arteries. Arrowheads indicate upper and lower boundary of the subendothelial matrix. Bars = 0.2 μm. C: distribution of subendothelial matrix layer thickness measured within the common carotid artery region of C57BL6 and apoE*3 mice (data from 41 and 63 micrographs, respectively) and the internal carotid artery sinus region of C57BL6 and apoE*3 mice (data from 51 and 39 micrographs, respectively). Values are means (SD). Difference in glycocalyx thickness between carotid artery regions of C57BL6 and apoE*3 mice was assessed by means of 2-sample *t*-test (2 way). **P* < 0.05 vs. C57BL6, common carotid region.



However, although studies have recently demonstrated that the endothelial glycocalyx indeed plays an important role in mechanotransduction of fluid shear stress, no data are available on the relation between fluid shear stress and glycocalyx synthesis (6, 7, 15).

In addition to the spatial differences in glycocalyx dimension, we also report that the glycocalyx is diminished in atherogenic mice on a high-fat, high-cholesterol diet. In line with the spatial relation between glycocalyx dimension and regional atherogenic risk, systemic perturbation of the glycocalyx by hypercholesterolemia and/or hypertriglyceremia introduced similar increases in vascular vulnerability. The mechanism by which the glycocalyx is diminished in atherogenic mice remains to be elucidated, but the present finding is consistent with previous studies demonstrating rapid shedding of glycocalyx from the endothelial surface on acute stimulation with elevated plasma levels of oxidized LDL or by acute exposure of the endothelium to inflammatory agents like thrombin or TNF- α (4, 12, 20).

Glycocalyx dimension and IMR. Previous studies demonstrated that loss of glycosaminoglycans from the endothelial glycocalyx by enzyme treatment is associated with edema formation of the subendothelial space (21), indicating that flow profile-related modulation of the glycocalyx might contribute to the earlier observed progression from a decreased endothelial barrier function into subsequent intimal edema at vascular regions exposed to disturbed flow (8). Whether edema formation contributed to the increased IMR in the present study remains to be explored. However, the site-specific differences and diet-induced increases in IMR occurred in the absence of changes in the dimension of the media layer and were predominantly due to respective differences and increases in the dimension of the subendothelial space. Furthermore, no evidence was found for accumulation of blood cells or monocytes in the intima layer, indicating that the contribution of the inflammatory response was minimal at this stage.

Study limitations. To ensure an unobstructed perfusion during staining, blood was removed with a solution containing both bovine serum albumin and a low dose of heparin. Because we cannot fully exclude possible interactions of heparin with proteins and carbohydrates within the endothelial glycocalyx layer, loss of glycocalyx components during this procedure must be considered. The present findings, although possibly lower for all regions, still allow comparison between the various regions of interest. Furthermore, the present dimensions of the common carotid and internal carotid flow divider artery region are still consistent with previous electron (without heparin) and intravital microscopic estimates (11, 21, 23).

In conclusion, atherosclerotic lesions develop at predisposed vascular regions and under conditions of elevated atherosclerotic risk. In the present study we demonstrate that the morphology and dimension of the endothelial cell glycocalyx are dramatically modified at atherogenic risk areas and by atherogenic high-fat diet. Small glycocalyx dimensions therefore reflect vulnerable endothelium, which is further supported by the increased IMR at these sites.

Although the current study does not prove causality of glycocalyx perturbation in development of intima thickening, it may stimulate further research to investigate the relation between atherogenic glycocalyx changes and loss of the protec-

tive properties of vascular endothelium against the development of atherosclerotic lesions.

ACKNOWLEDGMENTS

Present address of B. M. van den Berg: Department of Molecular and Vascular Medicine, Beth Israel Deaconess Medical Center, 330 Brookline Ave, Boston, MA 02215 (bvandenb@bidmc.harvard.edu).

GRANTS

This work was supported by the Netherlands Organization for Scientific Research (NWO no. 902-16-192) and a research fellowship from the Royal Netherlands Academy of Arts and Sciences (KNAW) to H. Vink.

REFERENCES

- Allen PL, Mowbray PI, Lee AJ, and Fowkes FG. Relationship between carotid intima-media thickness and symptomatic and asymptomatic peripheral arterial disease: the Edinburgh Artery Study. *Stroke* 28: 348–353, 1997.
- Bozzola JJ and Russel LD. Interpretation of microphotographs. In: *Electron Microscopy: Principles and Techniques for Biologists*. Boston, MA: Jones and Bartlett, 1992, p. 377–404.
- Clough G. Relationship between microvascular permeability and ultrastructure. *Prog Biophys Mol Biol* 55: 47–69, 1991.
- Constantinescu AA, Vink H, and Spaan JAE. Endothelial cell glycocalyx modulates immobilization of leukocytes at the endothelial surface. *Arterioscler Thromb Vasc Biol* 23: 1541–1547, 2003.
- Curry FE. Determinants of capillary permeability: a review of mechanisms based on single capillary studies in the frog. *Circ Res* 59: 367–380, 1986.
- Davies PF. Flow-mediated endothelial mechanotransduction. *Physiol Rev* 76: 519–560, 1995.
- Florian JA, Kosky JR, Ainslie K, Pang Z, Dull RO, and Tarbell JM. Heparan sulfate proteoglycan is a mechanosensor on endothelial cells. *Circ Res* 93: e136–e142, 2003.
- Fry DL. Arterial intimal-medial permeability and coevolving structural responses to defined shear-stress exposures. *Am J Physiol Heart Circ Physiol* 283: H2341–H2355, 2002. [Corrigenda. *Am J Physiol Heart Circ Physiol* 284: February 2003, following table of contents].
- Gorog P and Born GVR. Uneven distribution of sialic acids on the luminal surface of aortic endothelium. *Br J Exp Pathol* 64: 418–424, 1983.
- Haldenby KA, Chappell DC, Winlove CP, Parker KH, and Firth JA. Focal and regional variations in the composition of the glycocalyx of large vessel endothelium. *J Vasc Res* 31: 2–9, 1994.
- Hem A, Smith AJ, and Solberg P. Saphenous vein puncture for blood sampling of the mouse, rat, hamster, gerbil, guinea pig, ferret and mink. *Lab Anim* 32: 364–368, 1998.
- Henry CB and Duling BR. TNF- α increases entry of macromolecules into luminal endothelial cell glycocalyx. *Am J Physiol Heart Circ Physiol* 279: H2815–H2823, 2000.
- Liepsch D. An introduction to biofluid mechanics—basic models and applications. *J Biomech* 35: 415–435, 2002.
- Lutgens E, Daemen M, Kockx M, Doevendans P, Hofker M, Havekes L, Wellens H, and deMuninck ED. Atherosclerosis in APOE*3-Leiden transgenic mice. From proliferative to atheromatous stage. *Circulation* 99: 276–283, 1999.
- Mochizuki S, Vink H, Hiramatsu O, Kajita T, Shigeto F, Spaan JAE, and Kajiyama F. Role of hyaluronic acid glycosaminoglycans in shear-induced endothelium-derived nitric oxide release. *Am J Physiol Heart Circ Physiol* 285: H722–H726, 2003.
- Nishina PM, Verstuyft J, and Paigen B. Synthetic low and high fat diets for the study of atherosclerosis in the mouse. *J Lipid Res* 31: 859–869, 1990.
- O’Leary DH, Polak JF, Kronmal RA, Kittner SJ, Bond MG, Wolfson SK Jr, Bommer W, Price TR, Gardins JM, and Savage PJ. Distribution and correlates of sonographically detected carotid artery disease in the Cardiovascular Health Study. *Stroke* 23: 1752–1760, 1992.
- Poli A, Tremoli E, Colombo A, Sirtori M, Pignoli P, and Paoletti R. Ultrasonographic measurement of the common carotid artery wall thickness in hypercholesterolemic patients: a new model for the quantitation and follow-up of preclinical atherosclerosis in living human subjects. *Atherosclerosis* 70: 253–261, 1988.

19. **Sary HC, Blankenhorn DH, Chandler AB, Glagov S, Insull W Jr, Richardson M, Rosenfeld ME, Schaffer SA, Schwartz CJ, Wagner WD, and Wissler RW.** A definition of the intima of human arteries and of its atherosclerosis-prone regions. A report from the Committee on Vascular Lesions of the Council on Arteriosclerosis, American Heart Association. *Arterioscler Thromb* 12: 120–134, 1992.
20. **Subramanian SV, Fitzgerald ML, and Bernfield M.** Regulated shedding of syndecan-1 and -4 ectodomains by thrombin and growth factor receptor activation. *J Biol Chem* 272: 14713–14720, 1997.
21. **Van den Berg BM, Vink H, and Spaan JAE.** The endothelial glycocalyx protects against myocardial edema. *Circ Res* 92: 592–594, 2003.
22. **Van den Maagdenberg AM, Hofker MH, Krimpenfort PJ, de Bruijn I, van Vlijmen B, van der Boom H, Havekes LM, and Frants RR.** Transgenic mice carrying the apolipoprotein E3-Leiden gene exhibit hyperlipoproteinemia. *J Biol Chem* 268: 10540–10545, 1993.
23. **Vink H and Duling BR.** Identification of distinct luminal domains for macromolecules, erythrocytes, and leukocytes within mammalian capillaries. *Circ Res* 79: 581–589, 1996.
24. **Zarins CK, Giddens DP, Bharadvaj BK, Sottiurai VS, Mabon RF, and Glagov S.** Carotid bifurcation atherosclerosis. Quantitative correlation of plaque localization with flow velocity profiles and wall shear stress. *Circ Res* 53: 502–514, 1983.

